

# Near-Field Radiation Exposure Control in Slot-Loaded Microstrip Antenna: A Characteristic Mode Approach

Sandip Ghosal, Arijit De, Raed M. Shubair, and Ajay Chakrabarty

## Abstract

Microstrip antenna topology is commonly loaded with a narrow slot to manipulate the resonance frequency or impedance bandwidth. However, the tuning of the resonance frequency or impedance bandwidth results in the variation of the current and field distributions. In this regard, this work adopts the concept of characteristic modes to gain an initial understanding of the perturbation mechanism of the rectangular patch when loaded with a slot. The performance of microstrip antennas with finite ground plane is then studied using full-wave simulation. It has been found that the distribution of the induced current density is highly dependent on the orientation of the slot. The incorporation of a narrow slot suppresses the nearby orthogonal eigen mode and, as a consequence, the radiation behaviour is affected. Specifically, in the presence of biological tissues in the near-field region, both antenna input impedance properties and the realized gain are dependent on the slot orientation. Different examples are included for understanding the impact of slot loading on the energy absorption by biological tissues, by calculating the the specific absorption rate (SAR). The proposed analysis facilitates the design of miniaturized antenna geometries for biomedical applications via systematic loading of narrow slots.

S. Ghosal, A. De and A. Chakrabarty are with the Department of Electronics and Electrical Communication Engineering, Indian Institute of Technology, Kharagpur, West Bengal 721302, India (e-mail: sgmw@iitkgp.ac.in).

Raed M. Shubair is with Research Laboratory of Electronics, Massachusetts Institute of Technology (MIT), Cambridge, MA 02139 USA (e-mail: rshubair@mit.edu).

## I. INTRODUCTION

The last two decades have witnessed an exponential growth and tremendous developments in antenna technologies and techniques, and their associated applications, such as those reported in [1]–[44]. Being an integral part of the cellular phone, antenna's near-field exposure on biological tissues is a major concern for the antenna designers. RF exposure induced by the GSM mobile phone has been studied using statistical modelling in [45]. A numerical technique has also been proposed to determine the RF exposure effects on a human head due to a cellphone equipped with a dual-band monopole-helix antenna [46]. In a similar way, various statistical and experimental studies were carried out to assess the impact of mobile radiation on nearby biological tissues [47] [48] [49]. Recently, modal analysis technique has been adopted for predicting the frequency of maximum RF exposure [50] [51]. Therefore, the antenna geometry should be designed in a way such that it maintains a certain threshold of RF energy absorption by the biological tissues commonly characterized by the SAR value [52] [53].

Antenna design in the presence of nearby biological tissues involves three main aspects. The first is to select the optimum frequency for maximum power transfer, as rigorously studied in [54]. The second is to focus the radiated field or SAR distribution towards a desired direction [55] [56]. The third and last aspect, is to miniaturize the design while maintaining the desired radiation characteristics in the desired frequency of operation. Miniaturization of the design is achieved by incorporating electromagnetic band gap (EBG) structures [57] or slot elements [58] in the topology of the antenna. The latter technique is the focus of this report.

Slot loading of is a popular technique used by the antenna designers to manipulate resonance frequency [59], enhance impedance bandwidth [60], or reduce side-lobe level [61]. The principle behind slot loading technique is to manipulate the radiation behaviour which is directly controlled by the current density vector induced on the surface or volume of the radiating antenna. In this regard, a proper analysis is required to study the effect of slot loading on the radiated field and SAR. In the literature, slot loading phenomena has been discussed following three approaches: cavity modelling [61], method of moment (MoM) technique [62], and transmission line theory [58]. Recently, a modal approach based on characteristic mode analysis (CMA) has been employed to study the effect of slot loading [63] [64]. Characteristic mode theory was initially developed to determine the induced current vector using generalized eigen-decomposition of the MoM impedance matrix. If Galerkin's method is followed in the electric field integral equation (EFIE) formulation, the MoM impedance matrix becomes symmetric [65]. Generalized characteristic equation of

the MoM matrix provides the eigen-values and the characteristic current eigen-modes. As shown in [65] and [51], these eigen-values can predict the resonance frequency of the antenna structure. The amount of outward radiated power is also directly dependent on the eigen-modes and eigen-values. Unlike the conventional MoM technique, computation of these eigen parameters is independent of the excitation vector. It depends only on the operating frequency, and on the physical and geometrical properties of the radiating structure. Hence, with the knowledge of excitation-independent eigen-current distribution, one can perturb the radiating structure topology to achieve a desired radiation pattern. Such advantageous scopes of the CMA are found to be recently exploited in controlling the higher order modes [66] and radar cross section [67] respectively. This report aims to extend the previously reported modal approach of [63] [64], for perturbing the horizontal radiation in the near field of the radiating structure, such that the RF exposure on the on the nearby biological tissues is adjusted.

The report is organized as follows: Section II starts by describing the characteristic mode analysis, then considers a rectangular geometry to study the perturbation of modal current density due to the loading of narrow slots. Section III explores the method further with full-wave examples and corresponding analysis of the SAR distribution Finally, conclusions are given in Section IV..

## II. MODAL ANALYSIS

For the sake of initial understanding, let us consider a perfect electrically conducting (PEC) radiating element with no internal resonance. The outward unit vector normal to the surface of the antenna is denoted by  $\hat{n}$ .  $E^i$  is the excitation field vector of the antenna.  $J$  is the surface current density vector induced on the surface  $S$  of the antenna. Following the field boundary conditions on the surface  $S$  [65],

$$\hat{n} \times E^i = -\hat{n} \times [j\omega A(J(r')) + \nabla\phi(J(r'))] \quad (1a)$$

$$A(J(r')) = \mu \oint_S J(r') G(r, r') ds \quad (1b)$$

$$\phi(J(r')) = \frac{-1}{j\omega\epsilon} \oint_S \nabla' J(r') G(r, r') ds \quad (1c)$$

$$G(r, r') = \frac{e^{-jk|r-r'|}}{4\pi|r-r'|} \quad (1d)$$

The permittivity, permeability and wave-number of the free-space medium are represented by  $\mu$ ,  $\epsilon$  and  $k$  respectively. The integral equation of (1a)-(1d) can be converted into equivalent matrix form using the method of moment (MoM) technique [65] as,

$$[Z]_{M \times M} [I]_{M \times 1} = [V]_{M \times 1} \quad (2)$$

The MoM impedance matrix is denoted by  $[Z]$  and the column vector  $[V]$  consists of the weighting coefficients generated due to the inner product of the excitation vector  $E^i$  and  $M$  number of basis functions  $f_m$ . Using the CMA of [65], the weighting vector  $[I]$  of the induced current can be written as

$$[I] = \sum_{m=1}^M \alpha_m [I_m], \text{ where } \alpha_m = \frac{[I_m]^H [V]}{(1 + j\lambda_m) [I_m]^H [R] [I_m]} \quad (3)$$

and the  $m^{th}$  characteristic current mode  $J_m$  will be

$$J_m = \sum_{i=1}^M I_m(i) f_i(r'_m), r'_m \in S \quad (4)$$

The  $m^{th}$  eigenvector  $[I_m]$  and eigenvalue  $\lambda_m$  can be obtained through the generalised eigen decomposition of the impedance matrix  $[Z]$  as,

$$[X][I_m] = \lambda_m [R][I_m], \text{ where } [Z] = [R] + j[X] \quad (5)$$

If Galerkin's matching is followed in computing the  $[Z]$  matrix, both  $[R]$  and  $[X]$  will be real symmetric. So the eigen pair  $([I_m], \lambda_m)$  of (5) will be necessarily real valued. However it can be noted from [51] that

the lossy structures will have complex eigenvectors and eigenvalues. Following the orthogonal properties of the eigenvectors of (5), it can be written that

$$[I_m]^H [R] [I_n] = \delta_{mn} [I_m]^H [R] [I_m] \quad (6a)$$

$$[I_m]^H [X] [I_n] = \lambda_m \delta_{mn} [I_m]^H [R] [I_m] \quad (6b)$$

$$\delta_{mn} = 1 \text{ if } m = n, \text{ else } 0 \quad (6c)$$

The Hermitian transpose operation is denoted by ‘‘H’’. for the lossless structures, it will turn out to be as transposition operation. The modal significance of the  $m^{th}$  eigenmode is denoted by

$$MS_m = \frac{1}{\sqrt{1 + \lambda_m^2}}. \quad (7)$$

Following the complex -power balance relation of [65], the power radiated by the  $m^{th}$  mode can be defined as,

$$P_{R,m} = |\alpha_m|^2 = MS_m \left( \frac{[I_m]^H [V]}{[I_m]^H [R] [I_m]} \right)^2 \quad (8)$$

Total radiated power at a certain frequency, say,  $f_0$  will be a weighted sum of all individual modal power,

$$P_R = \sum_{m=1}^M P_{R,m} = \sum_{m=1}^M |\alpha_m|^2 \quad (9)$$

Now, let’s come back to the first two design objectives as stated in the initial part of the previous section. It can be noted from (8) that the outward radiated power  $P_{R,m}$  is inversely related to the eigenvalue  $\lambda_m$  of the corresponding mode. As  $\lambda_m$  tends towards 0, corresponding modal significance  $MS_m$  of (7) and radiated power  $P_{R,m}$  of (9) will be higher. Similarly when the antenna is used in the receiving end, real power of the pointing vectors provides  $P_{R,m}$  as the received real power. So, if the excitation vector is restricted to a very finite region compared to the total geometry of the antenna structure, the optimal frequency of maximum radiation can be approximated following the minima of the corresponding eigenvalue.

On the other hand, total radiated power consists of the contribution from all modes in (9). To align the field distribution along a certain direction or to achieve a desired SAR distribution, it is required to suppress the adjacent undesired modes. Let the  $i^{th}$  mode generates the desired beam pattern at the resonating frequency of  $\omega_i$ . Henceforth the desired radiated modal power is represented by  $|\alpha_m|^2$  where  $m = i$ . Alternately, the undesired component of the radiated power are contributed by the other additional modes,  $\sum_{m=1}^M |\alpha_m|^2$  for  $m \neq i$ . So the control over undesired radiation needs to start from the search of the characteristic mode(/s) whose modal radiated power is comparable to the desired mode’s power. Physically the eigenvalue parameter  $\lambda_i$  denotes the proximity towards resonance of the  $i^{th}$  characteristic

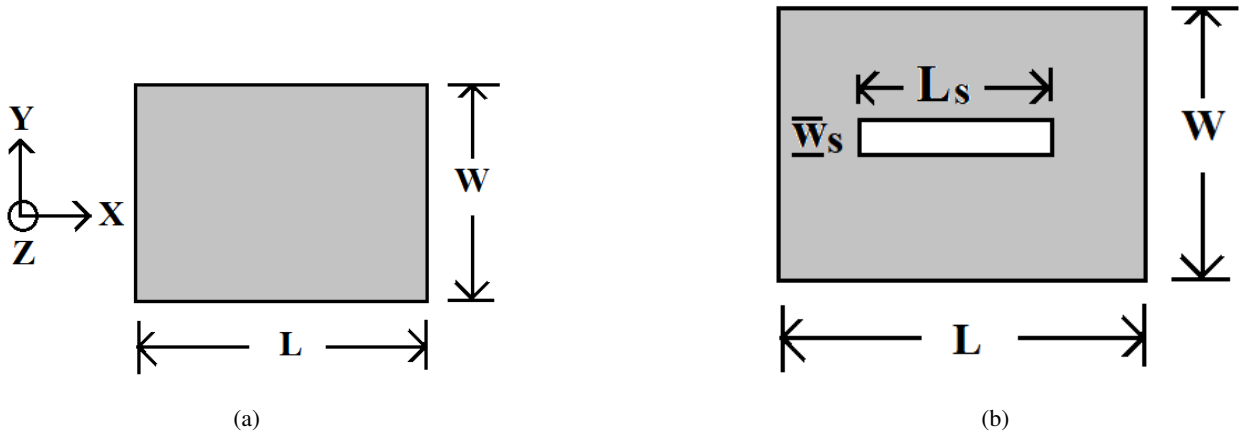


Fig. 1. (a) Reference plate with  $L = 50$  mm,  $W = 40$  mm. (b) The plate with narrow slot. For X-directed slot,  $L_s = 30$  mm and  $W_s = 0.2$  mm. For Y-directed slot,  $L_s = 0.2$  mm and  $W_s = 30$  mm.

mode. Ideal resonance criterion is defined by zero reactive power, in other words,  $\lambda_m = 0$ . So, the dominant eigenmodes are commonly determined using the modal significance parameter  $MS_m$  of (7). The next discussion shows how the modal characteristics vary due to loading of narrow slot. For the purpose of illustration, let us consider a rectangular PEC plate in Fig.1(a). The plate loaded with narrow slot is shown in Fig.1(b).

The eigenmodes have been computed in MATLAB [68] following [65] and [69] with RWG basis functions. Sorting the modes following (7), the 1<sup>st</sup> two dominant eigen current modes at  $f = 2.4$  GHz have been plotted in Figs.2(a) and 2(b). Keeping both the current distribution in same scale, the eigencurrent modes have been normalised with respect to its maximum amplitude. This leads to the presence of the additional term  $[I_m]^H [R] [I_m]$  in defining  $\alpha_m$  of (3). As shown in Figs.2(a) and 2(b), the 1<sup>st</sup> and 2<sup>nd</sup> eigenmodes are found to be linearly polarized along X and Y-direction respectively.

In the next stage, narrow slot has been incorporated with its wider axis along the X-direction where  $W_s = 0.2$  mm and  $L_s = 30$  mm. The perturbed current distribution of the first two dominant modes at  $f = 2.4$  GHz are shown in Figs. 2(c) and 2(d). Major contribution of the slot is reflected in the second mode of Fig. 2(d). It can be noted from the comparison between Fig.2(b) and 2(d) that the X-directed slot converts the nearest Y-polarized edge mode of Fig.2(b) into a slot mode of Fig.2(d) where the current distribution hold significant magnitude only along two narrow ends of the slot. The X-directed slot has minimal impact on the first mode in Fig.2(c) whose orientation is parallel to the wider axis of the slot. For studying the complementary case, the slot has been aligned along the Y-direction and the resultant modes have been shown in Figs. 2(e) and 2(f). Similar to the earlier case, the Y-polarised edge mode of Fig.2(a) is transformed into the Y-polarised edge mode in Fig.2(e). Minimal variation is noted in the

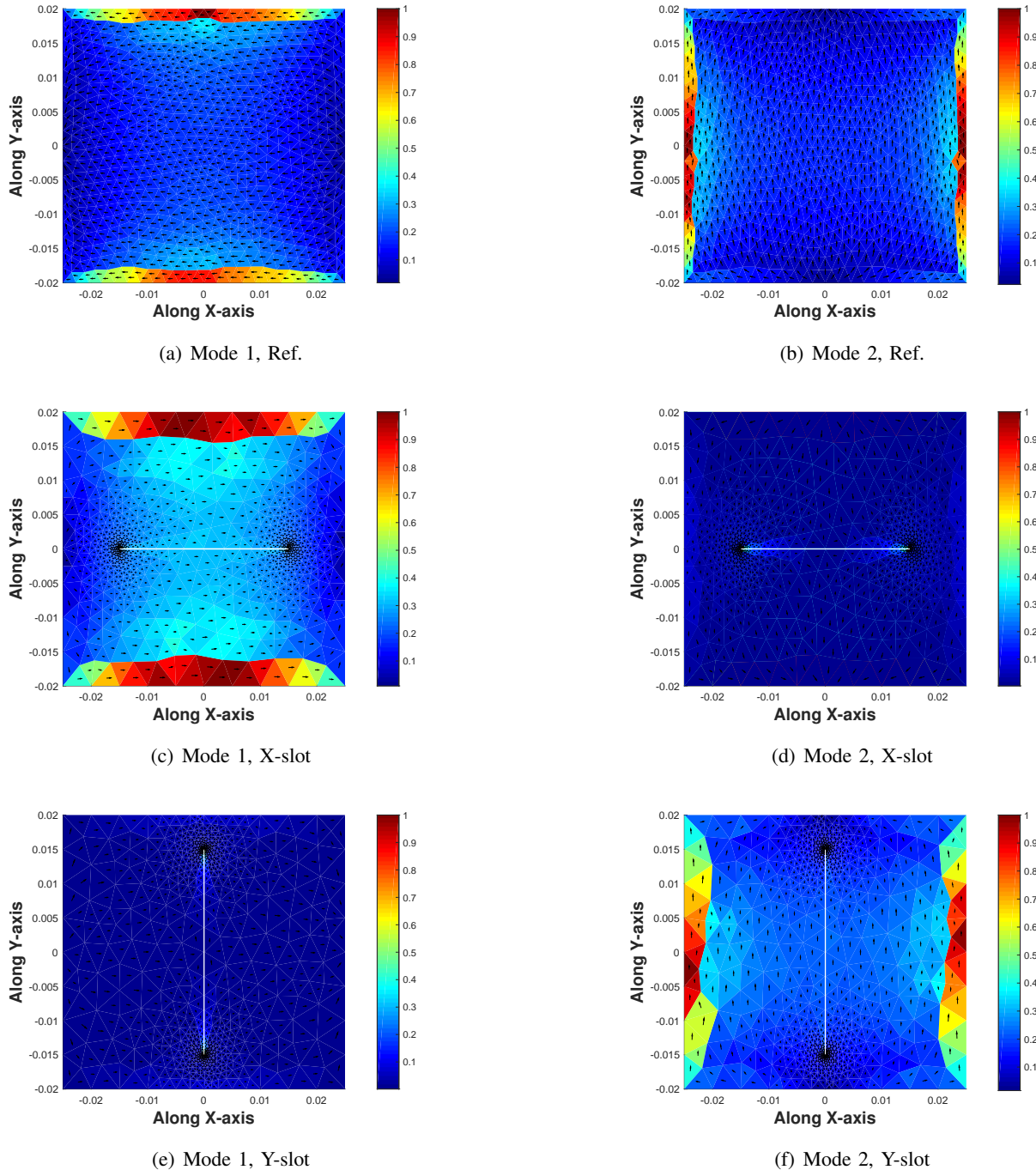


Fig. 2. Normalized distribution of the 1<sup>st</sup> and 2<sup>nd</sup> eigencurrent modes at  $f = 2.4$  GHz.

X-polarised edge mode of Fig.2(f).

As the loading of slot modify the current distribution, corresponding field distribution will also change.



Fig. 3. Field observation plane at  $z = 5$  mm height from the radiating plate.

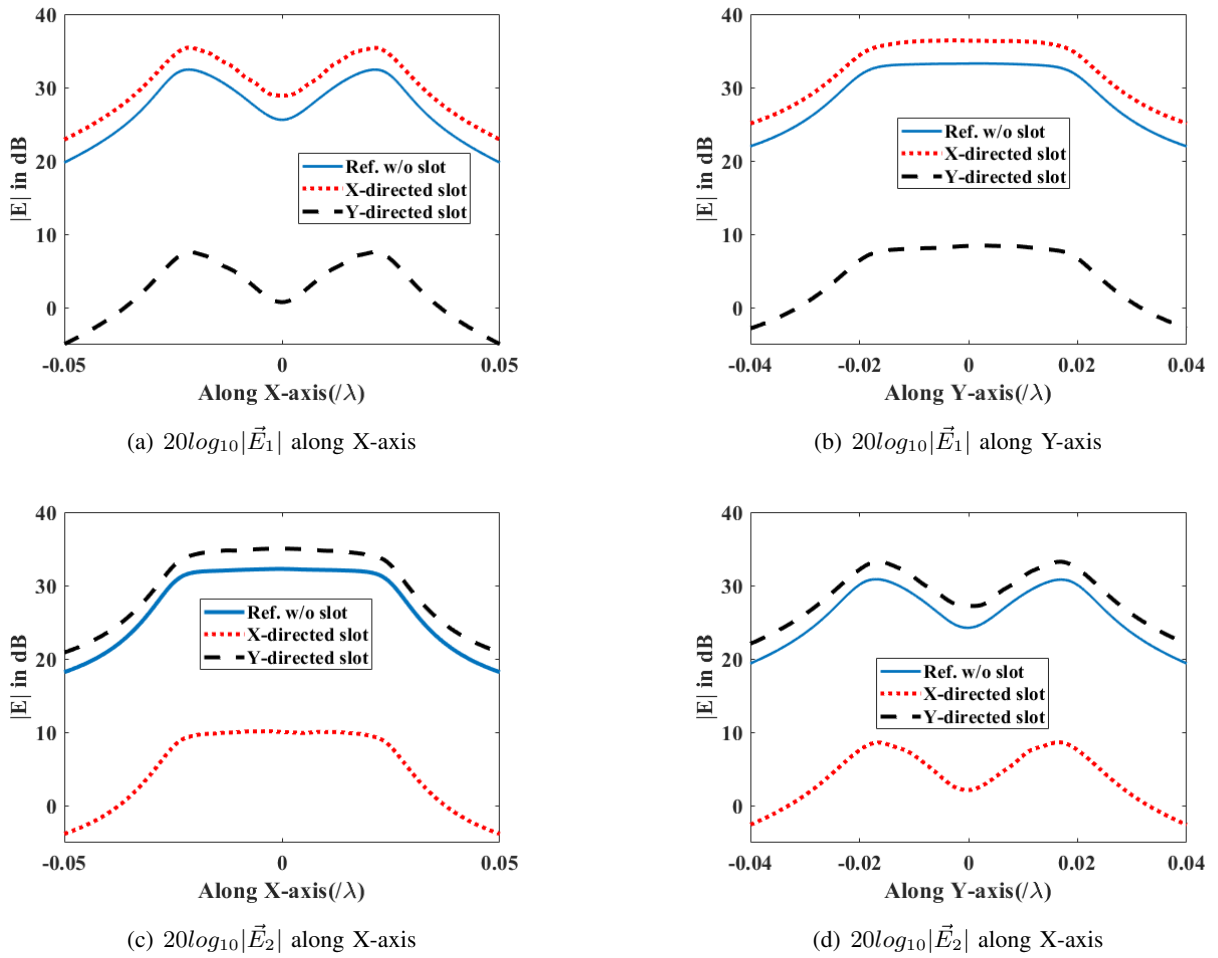


Fig. 4. Near field distribution due to the first two dominant characteristic current modes at  $f = 2.4$  GHz.

The SAR distribution on a nearby object is directly related to the electric field as

$$\text{SAR} = \frac{\sigma}{\rho} |\mathbf{E}|^2 \quad (10)$$

The nearby object will experience the incident field  $\mathbf{E}$  contributed by the antenna structure. For example



while holding a cell phone like Fig. II, the horizontal radiation will influence the biological tissues. To understand the impacts on the near field variation along the horizontal direction, let us consider a line of observation at an offset distance from the edges of the PEC plate (i.e., the radiating source). Using infinitesimal dipole model of [69], the electric field  $20\log_{10}|E|$  has been calculated for the corresponding eigencurrent modes. It can be noted from Figs. 4(a) and 4(b) that the X-directed slot enhances the X-polarised 1<sup>st</sup> mode's near field density whereas the Y-directed slot reduces the corresponding modal strength. Similarly, the Y-polarised mode is found to be weakened by the X-directed narrow slot in Figs. 4(c) and 4(d). Such variation in the near field behaviour due to loading of narrow slot will influence the SAR distribution of the neighbouring biological tissue following (10). Therefore, the radiating element can be suitably designed based the characteristic mode analysis to minimize the undesired radiation. Till now, the modal analysis does not consider the information of the excitation vector. The next section uses the same radiating elements of Figs. 1(a) and 1(b) with finite microstrip ground plane to verify the suitability of the slot loading method using full-wave simulator Ansys HFSS [70].

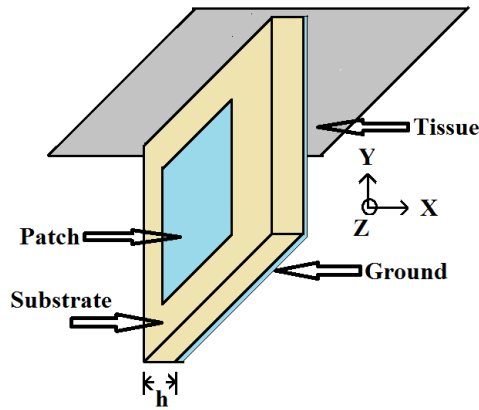


Fig. 5. Antenna with the adjacent tissue layer.

### III. FULL-WAVE ANALYSIS

For the full-wave study, two different case studies have been considered with probe-feeding and microstrip line feeding arrangement. For each case, the patch dimensions have been assumed to be same as of Figs. 1(a) and 1(b). The patch surface is lying 1.57 mm above the lossless Roger substrate with the dielectric permittivity of 2.2. The tissue is placed parallel to the XZ-plane with the Y-separation of 2 mm from the substrate edge of the antenna as shown in Fig. 5.

#### A. Probe-fed Patch

The dimension of the ground plane is assumed to be 83.6 mm  $\times$  71.5 mm for tuning the reference antenna around 2.4 GHz using Ansys Design Kit. The antenna has been excited by co-axial probe feeding at ( $x_f = 2$  mm,  $y_f = 8.05$  mm,  $z_f = 1.57$  mm). The current distribution induced on the patch surface of the reference antenna is shown in Fig. 6(a) where the current is found to be Y-polarised. Following the previous modal discussion, if it is desired to suppress this Y-polarised current density, the narrow slot needs to be aligned along the orthogonal direction, i.e., along the X-axis. So for the sake of comparison, two examples have been studied with the X-directed and Y-directed slots on the patch surface. The feed location has been taken as same of the reference probe-fed patch. As obvious in Fig. 6(a), the orthogonal orientation of the slot can perturb the Y-polarised edge mode of Fig. 6(a) into the slot mode. On the other hand, as the slot is oriented parallel to the Y-polarised edge mode, it has negligible impact on the current distribution in Fig. 6(c). As the slot perturbs the induced current density vector, the impedance characteristics also change in Fig. 6(d). The change in the equivalent circuit parameters can be computed using the existing analysis of [58] and [63]. The next discussion shows how the perturbation of the current vector becomes reflected in the near field and corresponding SAR distribution.

To understand the change in horizontal radiation, the near field at the same offset distance from two edges are reported in Figs. 7(a) and 7(b). Similar to the previous observation of Figs. 4(a)–4(d), the near field strength along the horizontal directed is found to be reduced due to loading of the narrow slot of orthogonal orientation. In the next stage, the tissue layer is placed parallel to the Y-edge of the antenna as shown in Fig. 5. The separation distance between the antenna and the tissue layer along the Y-axis is assumed to be 2 mm.

Following [52], the material properties of the tissue model have been given in Table I where the thickness of the corresponding layer is denoted by  $d$  in mm. The electrical conductivity, relative permittivity and mass density of the layers are denoted by  $\rho$ ,  $\epsilon_r$  and  $\sigma$  in Table I. Since the tissue layer is placed with very close electrical distance ( $0.016\lambda_0$ ,  $\lambda_0$  being the free-space wavelength at  $f = 2.4$  GHz) from the antenna element, it lies in the radiative near field region at  $f = 2.4$  GHz.

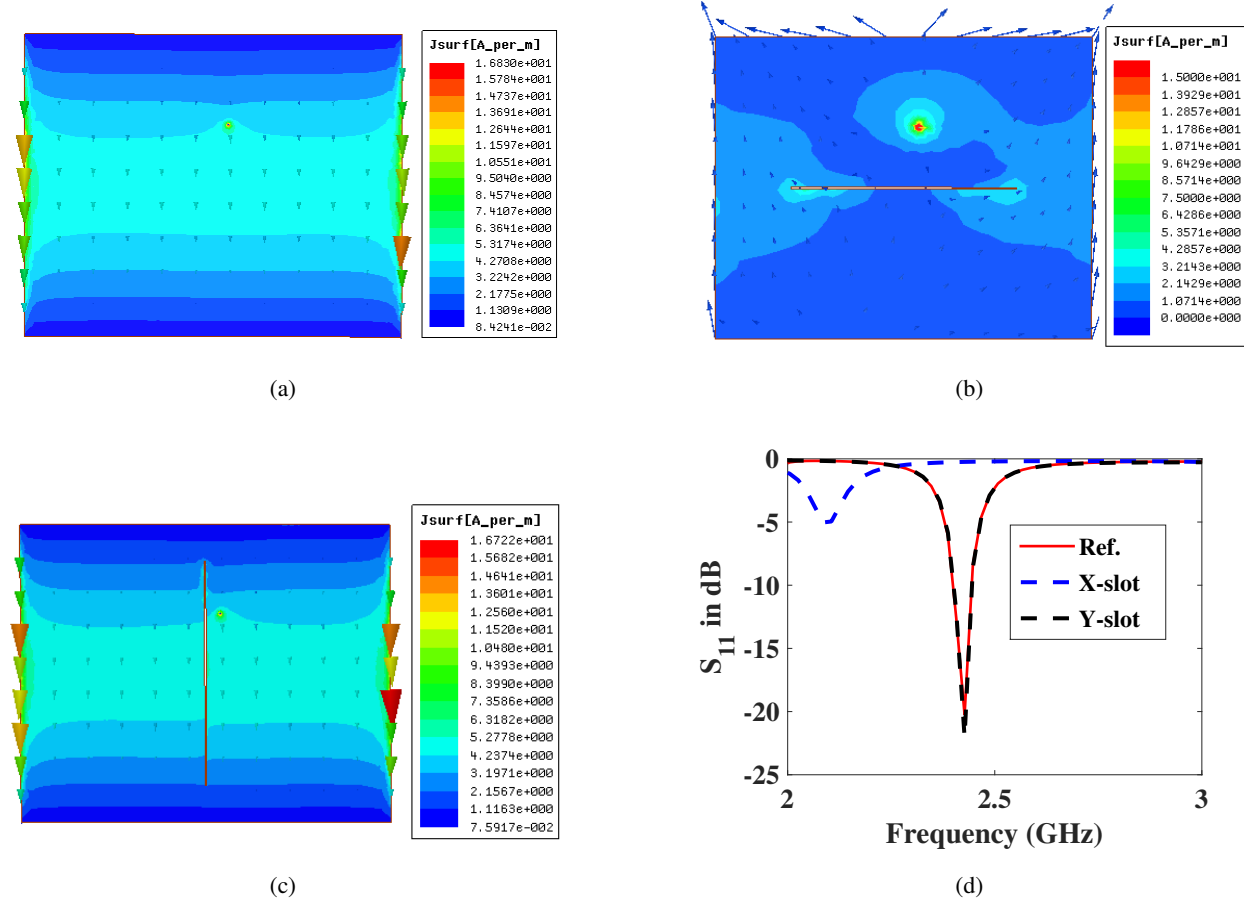


Fig. 6. Normalized distribution of the characteristic current modes at  $f = 2.4$  GHz. (c) 1<sup>st</sup> and (d) 2<sup>nd</sup> modes of the plate with X-directed slot.

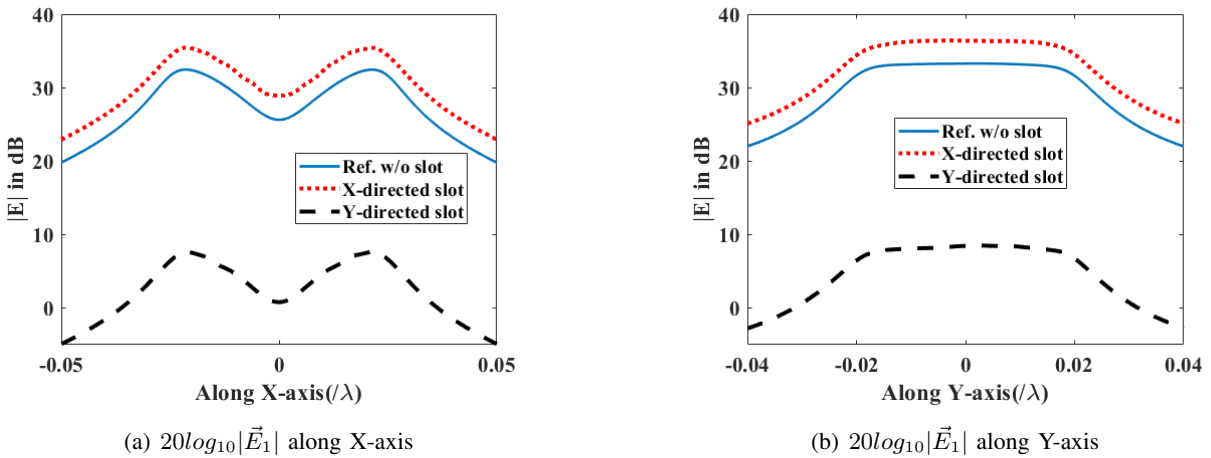


Fig. 7. Near field distribution due to the probe-fed patch at  $f = 2.4$  GHz.

Being placed at horizontal separation, the tissue will be coupled by the horizontal radiation components.

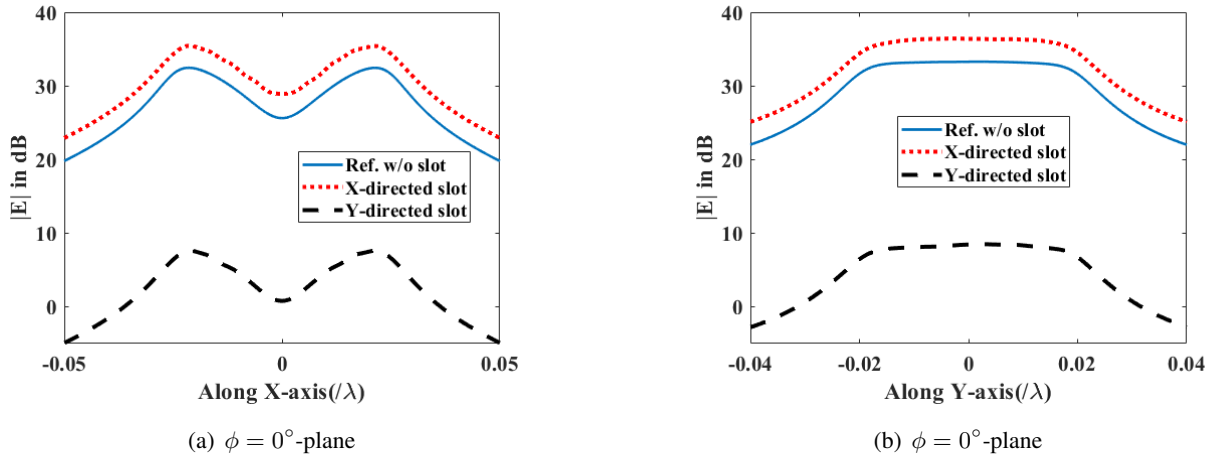


Fig. 8. Far field distribution due to the probe-fed patch at  $f = 2.4$  GHz.

TABLE I  
SPECIFICATION OF THE TISSUE LAYERS

Tissue	$\sigma(\text{S/m})$	$\epsilon_r$	$\rho(\text{kg/m}^3)$	d(mm)
skin	1.43	38.1	1100	1.5
fat	0.1	5.29	916	1.5

The electromagnetic exposure of the tissue layer can be characterised by specific absorption rate (SAR) parameter of (10). The incident field on the tissue is directly related to the induced characteristic modes of the antenna which vary its nature due to orientation of the narrow slot. The field emerging out of the radiating patch antenna will experience multiple reflection and scattering from the tissue layer. As a consequence, the SAR distribution on the tissue will be perturbed accordingly. Apart from the induced field  $\vec{E}_o$ , effective amount of the SAR value is also dependent on  $\rho$  and  $\sigma$ . For the case study, two different tissues-skin and fat have been considered. The SAR distribution for the probe-fed reference patch have been computed using Ansys HFSS and shown in Figs. 9(a)–9(f). It can be noted from the comparison of Figs. 9(a), 9(c), and 9(e) that the X-directed slot reduces the electromagnetic energy absorption compared to the reference antenna with no slot. The reason will be obvious from the preceding current distribution and near field distribution where the Y-directed slot suppresses the Y-polarised current distribution of the reference patch.

Alternately, the Y-directed slot enhances the Y-polarised mode. As a consequence, the SAR value is found to be slightly increased for the patch with the Y-directed slot. The slot mode nature leads to generate two concentric maxima regions in the skin layer of Fig. 9(c). Similar characteristics can be

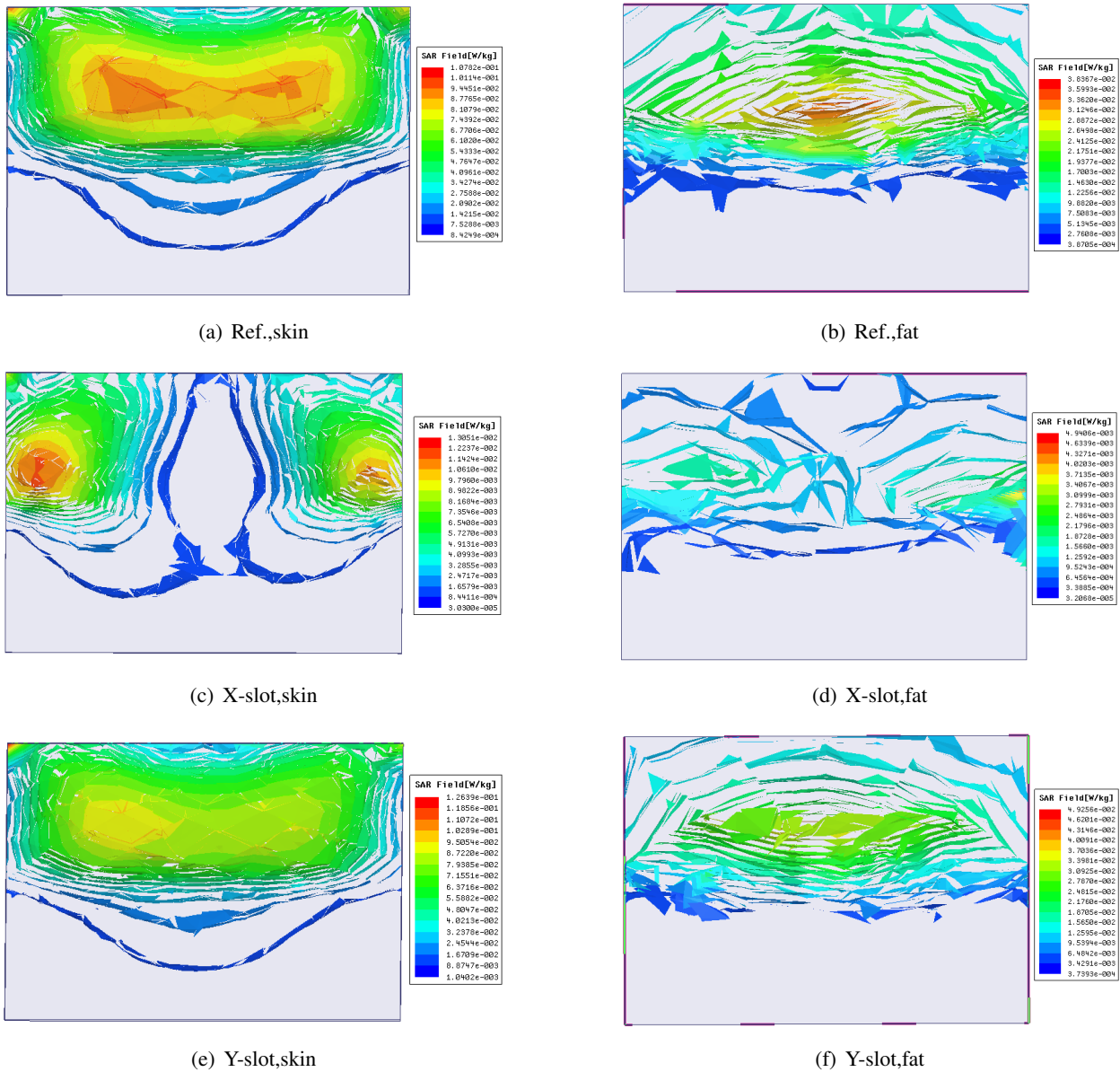


Fig. 9. SAR distribution for three probe-fed antenna topologies with two different tissue layers at  $f = 2.4$  GHz. Tissue is lying along the XZ-plane with the dimension of  $85 \text{ mm} \times 60 \text{ mm}$ .

TABLE II  
MAXIMUM SAR VALUE COMPARISON OF THE PROBE-FED PATCH

Tissue	$\frac{\max(SAR_{ref})}{\max(SAR_{X-slot})}$	$\frac{\max(SAR_{ref})}{\max(SAR_{Y-slot})}$
skin	8.23	0.8492
fat	7.77	0.78

found the examples with fat layer also. The SAR value is reduced by the X-directed slot and enhanced by the Y-directed slot. Maximum SAR values for the tissue layers have been compared in Table II for different orientation of the slot. The next discussion considers microstrip line fed patches for comparison.

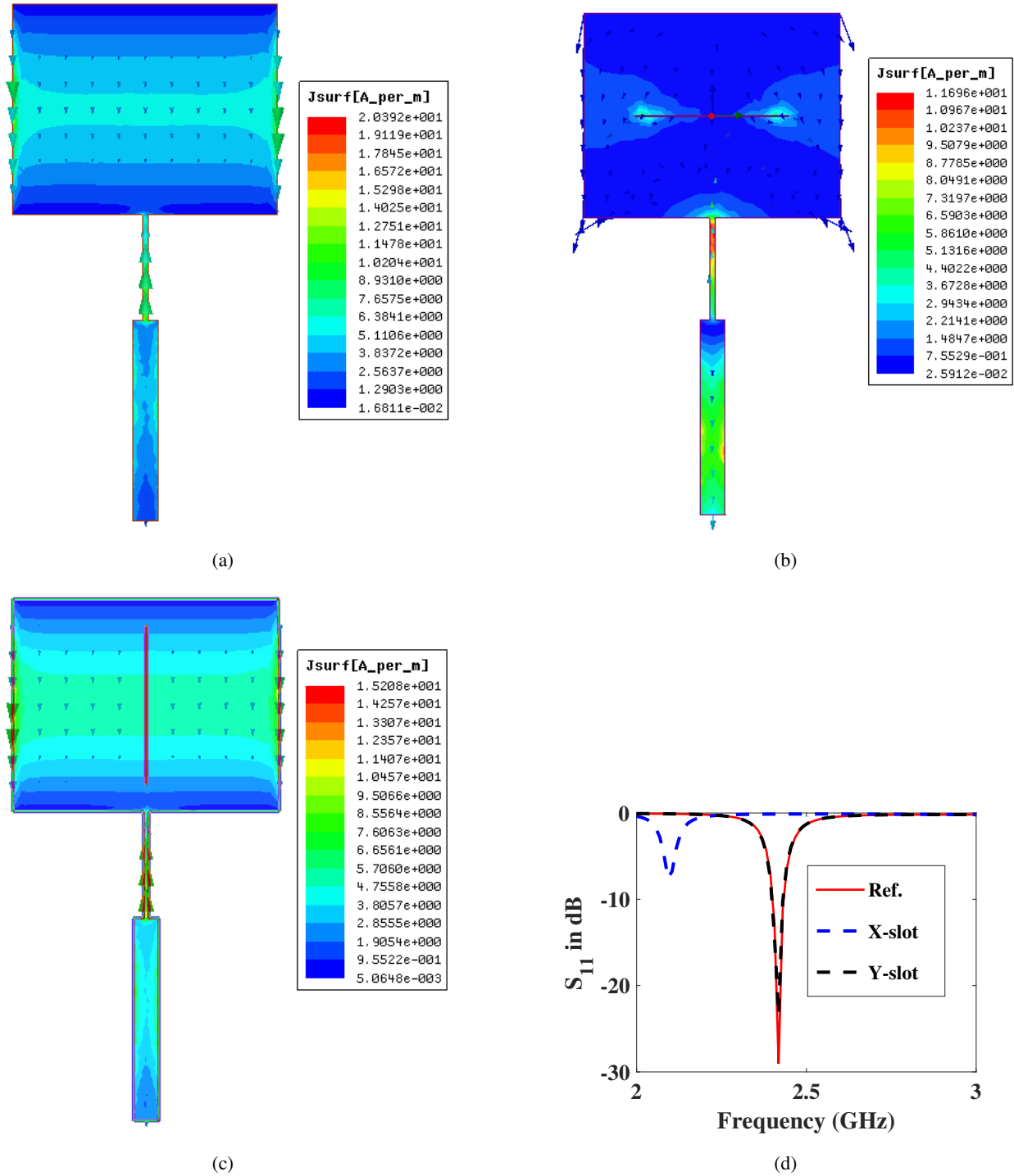


Fig. 10. Normalized distribution of the characteristic current modes at  $f = 2.4$  GHz. (c)  $1^{st}$  and (d)  $2^{nd}$  modes of the plate with X-directed slot.

### B. Microstrip line fed Patch

Similar patch elements have been considered but with microstrip line feeding arrangement. Using Ansys Design Kit, the feed-line of the reference antenna is tuned to 2.4 GHz with the same dimension of the radiating patch. The dimension of the ground plane is considered to be  $83.6 \text{ mm} \times 156 \text{ mm}$ . The current distribution have been compared in Figs. 10(a)–10(c). Similar to the probe-fed examples, the X-directed slot is found to suppress the Y-polarised edge mode of Fig. 10(a). The impedance matching behaviour is also influenced by the orientation of the slot in Fig. 10(d).

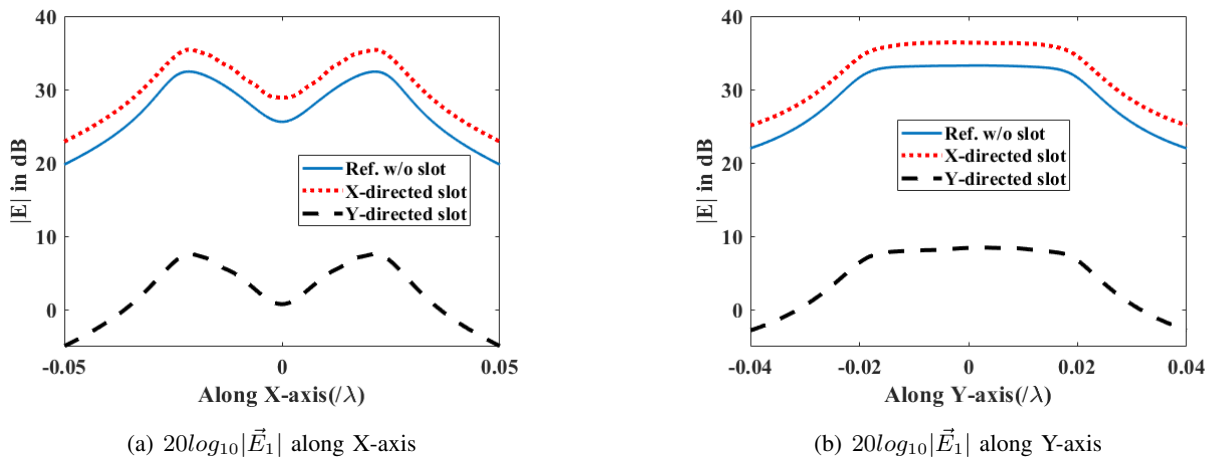


Fig. 11. Near field distribution due to the microstrip line-fed patch at  $f = 2.4 \text{ GHz}$ .

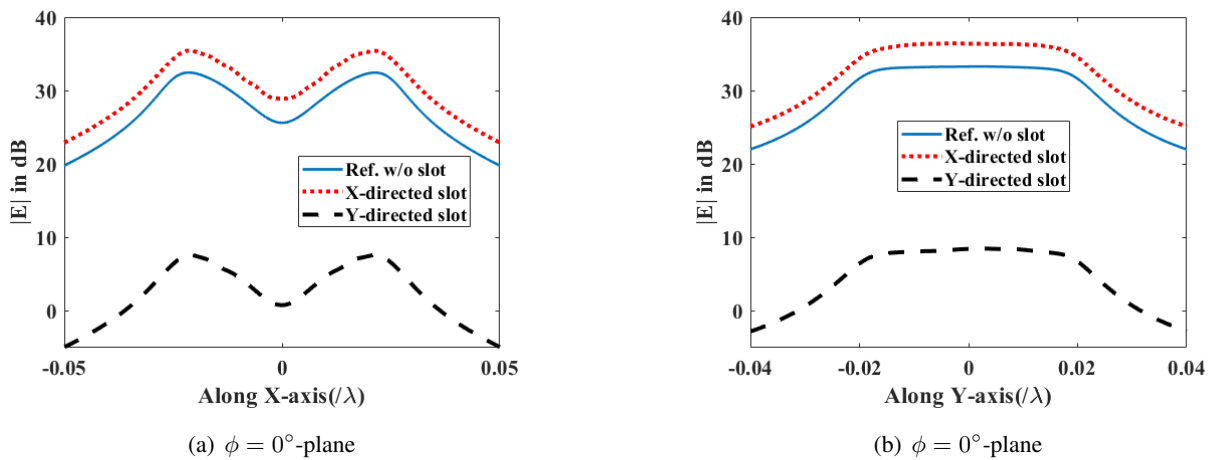


Fig. 12. Far field distribution due to the microstrip line-fed patch at  $f = 2.4 \text{ GHz}$ .

As shown in Figs. 11(a) and 11(b), the near field due to the horizontal radiation is also decreased by the orthogonal slot. Henceforth, the intuitive hints provided by the characteristic mode analysis is valid for both types of feeding arrangements.

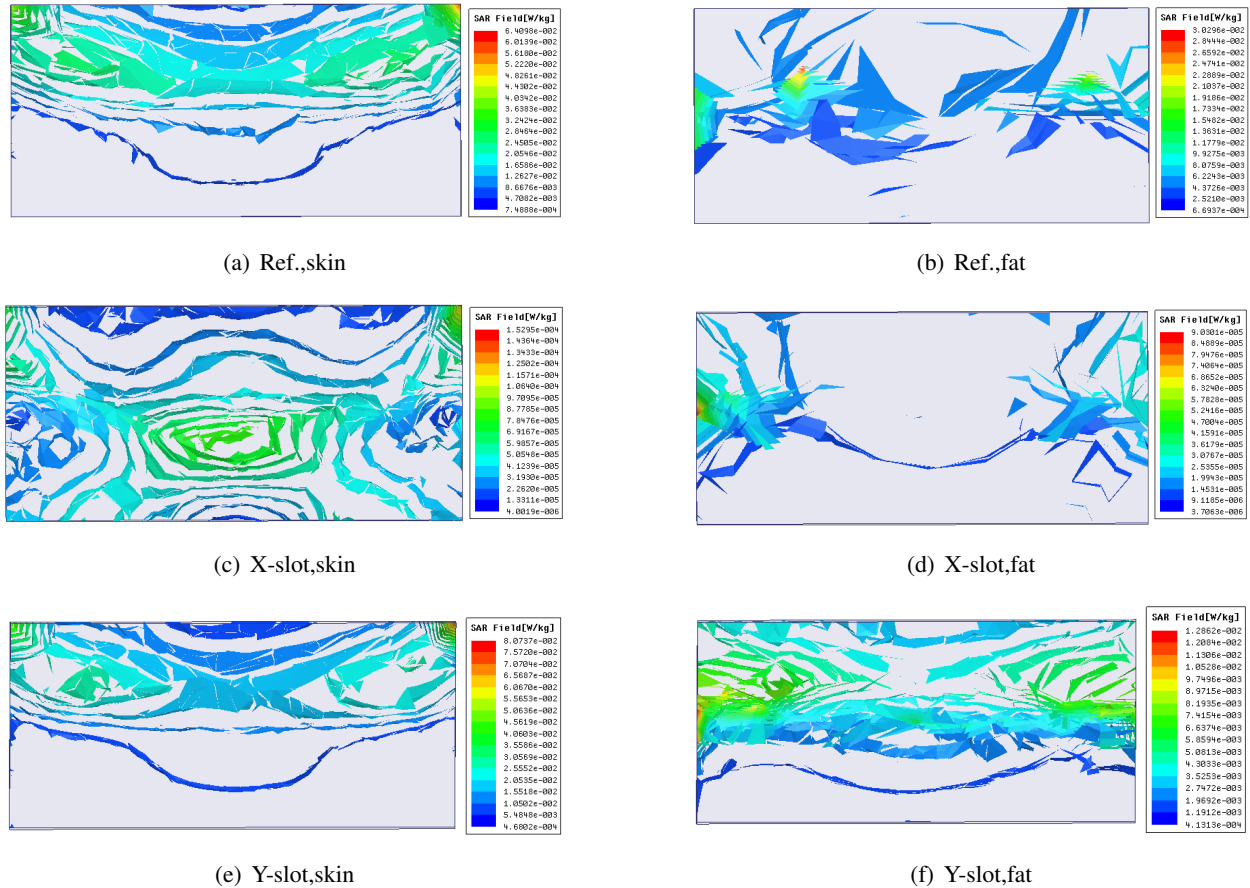


Fig. 13. SAR distribution for three line-fed antenna topologies with two different tissue layers at  $f = 2.4$  GHz. Tissue is lying along the XZ-plane with the dimension of  $85 \text{ mm} \times 40 \text{ mm}$ .

TABLE III  
MAXIMUM SAR VALUE COMPARISON OF THE LINE-FED PATCH

Tissue	$\frac{\max(SAR_{ref})}{\max(SAR_{X-slot})}$	$\frac{\max(SAR_{ref})}{\max(SAR_{Y-slot})}$
skin	418.3	0.79
fat	336.56	2.36

The impacts of the current perturbation on the resultant SAR distribution have been studied in Fig.13(a)–13(f) for both skin and fat tissue layers. As shown in Fig.13(c) and 13(d), the X-directed slot reduces the SAR value compared to the reference antennas of Fig.13(a) and 13(b). The nature of distribution is also changed as there appears a concentric maxima around the centre for the X-directed slot. However, for the Y-directed slot, other constitutive parameters like  $\sigma$  and  $\rho$  also control the variation of SAR following (10). As a consequence, the SAR value is enhanced by the Y-slot for the skin layer where as for the fat layer, it is slightly increased. Comparison of the maximum SAR values of the line fed antennas have



been reported in Table III. The impacts of X-directed slot is found to be maximum for the microstrip line feeding with respect to the probe feeding because the direction of the current in the feed line is parallel to the target Y-polarised edge mode of the antenna. So the modal weighting coefficient  $\alpha_n$  of (3) starts to be an influencing parameter. As two vectors  $[V]$  and  $[I_m]$  becomes parallel, their inner product holds higher value in the line fed antennas. Thus, both the radiating element's modal characteristics and the orientation of the excitation signal control the resultant radiation behaviour.

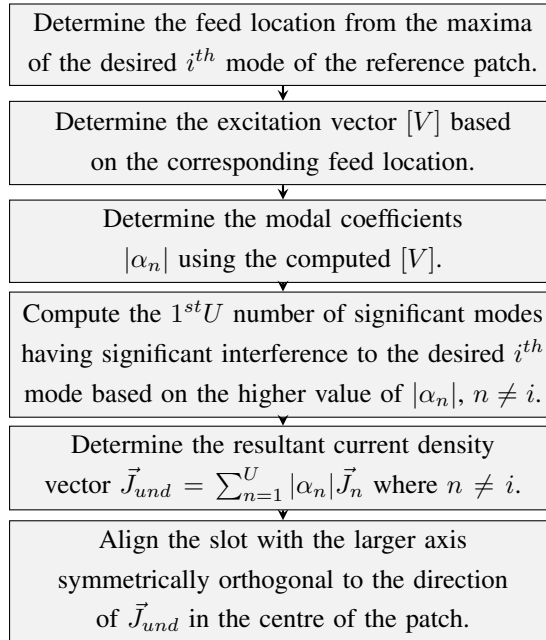


Fig. 14. Procedure for determining the orientation of the narrow slot.

In general, the characteristic mode analysis is found to provide systematic guideline for maintaining the radiated signal's polarization requirement and SAR distribution along a desired direction. For arbitrary orientation of the current distribution, the procedure of slot loading has been included in Fig. 14.

#### IV. CONCLUSION

This work explored the impacts of slot loading in rectangular patch antennas. Initially characteristic mode analysis of the radiating structures were performed to understand the perturbation in the current and field distribution. Later full-wave study had been carried out to investigate the loading effects on the electromagnetic energy absorption by biological tissues placed in the near field region. It was found that the prior knowledge of the characteristic modes of the radiating geometry can provide suitable information about the arrangement of the narrow slot for reducing the SAR value of the neighbouring tissues. The orientation of the slot is found to determine the amount of maximum radiation in a particular direction. Such important feature of the CMA can be further utilised for focussing the power of the wireless power transfer system to a target region of interest.

#### REFERENCES

- [1] H. Elayan, R. M. Shubair, J. M. Jornet, A. Kiourti, and R. Mittra, "Graphene-Based Spiral Nanoantenna for Intrabody Communication at Terahertz," in *2018 IEEE International Symposium on Antennas and Propagation USNC/URSI National Radio Science Meeting*, Jul. 2018, pp. 799–800.
- [2] H. Elayan, R. M. Shubair, and A. Kiourti, "On graphene-based THz plasmonic nano-antennas," in *2016 16th Mediterranean Microwave Symposium (MMS)*, Nov. 2016, pp. 1–3.
- [3] R. M. Shubair and Y. L. Chow, "A simple and accurate approach to model the coupling of vertical and horizontal dipoles in layered media," in *IEEE Antennas and Propagation Society International Symposium 1992 Digest*, Jun. 1992, pp. 2309–2312 vol.4.
- [4] A. A. Ibrahim and R. M. Shubair, "Reconfigurable band-notched UWB antenna for cognitive radio applications," in *2016 16th Mediterranean Microwave Symposium (MMS)*, Nov. 2016, pp. 1–4.
- [5] M. S. Khan, A. Capobianco, S. M. Asif, A. Iftikhar, B. D. Braaten, and R. M. Shubair, "A pattern reconfigurable printed patch antenna," in *2016 IEEE International Symposium on Antennas and Propagation (APSURSI)*, Jun. 2016, pp. 2149–2150.
- [6] R. M. Shubair, A. Salah, and A. K. Abbas, "Novel implantable miniaturized circular microstrip antenna for biomedical telemetry," in *2015 IEEE International Symposium on Antennas and Propagation USNC/URSI National Radio Science Meeting*, Jul. 2015, pp. 947–948.
- [7] S. Alharbi, R. M. Shubair, and A. Kiourti, "Flexible Antennas for Wearable Applications: Recent Advances and Design Challenges," in *12th European Conference on Antennas and Propagation (EuCAP 2018)*, Jan. 2018.
- [8] O. M. Khan, Q. U. Islam, R. M. Shubair, and A. Kiourti, "Novel multiband Flamenco fractal antenna for wearable WBAN off-body communication applications," in *2018 International Applied Computational Electromagnetics Society Symposium (ACES)*, Mar. 2018, pp. 1–2.
- [9] M. S. Khan, A. Capobianco, S. M. Asif, A. Iftikhar, B. D. Braaten, and R. M. Shubair, "A properties comparison between copper and graphene-based UWB MIMO planar antennas," in *2016 IEEE International Symposium on Antennas and Propagation (APSURSI)*, Jun. 2016, pp. 1767–1768.
- [10] S. Ghosal, A. De, A. Chakrabarty, and R. M. Shubair, "Characteristic Mode Analysis of Slot Loading in Microstrip Patch Antenna," in *2018 IEEE International Symposium on Antennas and Propagation USNC/URSI National Radio Science Meeting*, Jul. 2018, pp. 1523–1524.
- [11] O. M. Khan, R. M. Shubair, and Q. U. Islam, "Second order flamenco fractal antenna for industrial scientific and medical applications," in *2017 International Conference on Electrical and Computing Technologies and Applications (ICECTA)*, Nov. 2017, pp. 1–3.

- [12] M. S. Khan, A. Iftikhar, A.-D. Capobianco, R. M. Shubair, and B. Ijaz, "Pattern and frequency reconfiguration of patch antenna using PIN diodes," *Microwave and Optical Technology Letters*, vol. 59, no. 9, pp. 2180–2185, 2017. [Online]. Available: <https://onlinelibrary.wiley.com/doi/abs/10.1002/mop.30709>
- [13] R. M. Shubair and Y. L. Chow, "Complex images of vertical antenna penetrating a dielectric half-space," in *Proceedings of IEEE Antennas and Propagation Society International Symposium*, Jun. 1993, pp. 1187–1190 vol.3.
- [14] R. A. Kipp and C. H. Chan, "A numerically efficient technique for the method of moments solution for planar periodic structures in layered media," *IEEE Transactions on Microwave Theory and Techniques*, vol. 42, no. 4, pp. 635–643, Apr. 1994.
- [15] O. M. Khan, R. M. Shubair, Q. U. Islam, and I. Rashid, "Triband Metamaterial Embedded Implantable Antenna for Biotelemetry Applications," in *2018 IEEE International Symposium on Antennas and Propagation USNC/URSI National Radio Science Meeting*, Jul. 2018, pp. 213–214.
- [16] R. Karli, H. Ammor, R. M. Shubair, M. I. A. Hajri, and A. Hakam, "Minituarized printed L-shaped antenna with parasitic element for ultra-wideband applicatons," in *2016 17th International Symposium on Antenna Technology and Applied Electromagnetics (ANTEM)*, Jul. 2016, pp. 1–2.
- [17] R. M. Shubair, "An optimized complex-image prediction model for a closed-form solution of vertical antennas above a dielectric half-space," in *1998 Symposium on Antenna Technology and Applied Electromagnetics*, Aug. 1998, pp. 283–286.
- [18] R. M. Shubair and Y. L. Chow, "A technique for the efficient computation of the periodic Green's function in layered dielectric media," in *1992 IEEE MTT-S Microwave Symposium Digest*, Jun. 1992, pp. 393–396 vol.1.
- [19] R. M. Shubair, Y. L. Chow, and J. J. Yang, "A full wave complex image solution of horizontal electric dipoles in a thick dielectric sheet," in *Antennas and Propagation Society Symposium 1991 Digest*, Jun. 1991, pp. 1372–1375 vol.3.
- [20] R. M. Shubair and Y. L. Chow, "Analysis of the coupling of vertical and horizontal dipoles in layered media," in *1992 Symposium on Antenna Technology and Applied Electromagnetics*, Aug. 1992, pp. 211–216.
- [21] —, "A combined complex image-induced EMF solution of vertical antennas above a dielectric half-space," in *Proceedings of IEEE Antennas and Propagation Society International Symposium*, Jun. 1993, pp. 1030–1033 vol.2.
- [22] —, "Complex images for the calculation of the electrostatic potential in multilayered media," in *Proceedings of IEEE Antennas and Propagation Society International Symposium*, Jun. 1993, pp. 166–169 vol.1.
- [23] R. Karli, H. Ammor, R. M. Shubair, M. I. AlHajri, R. Alkurd, and A. Hakam, "Miniature planar ultra-wide-band microstrip antenna for breast cancer detection," in *2016 16th Mediterranean Microwave Symposium (MMS)*, Nov. 2016, pp. 1–4.
- [24] R. M. Shubair and Y. Chow, "A simple and accurate complex image interpretation of vertical antennas present in contiguous dielectric half-spaces," *IEEE transactions on antennas and propagation*, vol. 41, no. 6, pp. 806–812, 1993.
- [25] —, "Efficient computation of the periodic green's function in layered dielectric media," *IEEE transactions on microwave theory and techniques*, vol. 41, no. 3, pp. 498–502, 1993.
- [26] M. S. Khan, A.-D. Capobianco, S. M. Asif, D. E. Anagnostou, R. M. Shubair, and B. D. Braaten, "A compact csrr-enabled uwb diversity antenna," *IEEE Antennas and Wireless Propagation Letters*, vol. 16, pp. 808–812, 2016.
- [27] R. Shubair and Y. Chow, "A closed-form solution of vertical dipole antennas above a dielectric half-space," *IEEE transactions on antennas and propagation*, vol. 41, no. 12, pp. 1737–1741, 1993.
- [28] M. Al-Nuaimi, R. Shubair, and K. Al-Midfa, "Direction of arrival estimation in wireless mobile communications using minimum variance distortionless response," in *The Second International Conference on Innovations in Information Technology (IIT05)*, 2005, pp. 1–5.
- [29] G. Nwalozie, V. Okorogu, S. Maduadichie, and A. Adenola, "A simple comparative evaluation of adaptive beam forming algorithms," *International Journal of Engineering and Innovative Technology (IJEIT)*, vol. 2, no. 7, 2013.
- [30] W. Che, C. Li, P. Russer, and Y. Chow, "Propagation and band broadening effect of planar integrated ridged waveguide in multilayer dielectric substrates," in *2008 IEEE MTT-S International Microwave Symposium Digest*. IEEE, 2008, pp. 217–220.
- [31] R. Shubair, "Robust adaptive beamforming using lms algorithm with smi initialization," in *2005 IEEE Antennas and Propagation Society International Symposium*, vol. 4. IEEE, 2005, pp. 2–5.
- [32] A. Omar and R. Shubair, "Uwb coplanar waveguide-fed-coplanar strips spiral antenna," in *2016 10th European Conference on Antennas and Propagation (EuCAP)*. IEEE, 2016, pp. 1–2.

- [33] M. Bakhar and D. P. Hunagund, "Eigen structure based direction of arrival estimation algorithms for smart antenna systems," *IJCSNS International Journal of Computer Science and Network Security*, vol. 9, no. 11, pp. 96–100, 2009.
- [34] M. S. Khan, A.-D. Capobianco, A. Iftikhar, R. M. Shubair, D. E. Anagnostou, and B. D. Braaten, "Ultra-compact dual-polarised uwb mimo antenna with meandered feeding lines," *IET Microwaves, Antennas & Propagation*, vol. 11, no. 7, pp. 997–1002, 2017.
- [35] R. M. Shubair, A. M. AlShamsi, K. Khalaf, and A. Kiourti, "Novel miniature wearable microstrip antennas for ism-band biomedical telemetry," in *2015 Loughborough Antennas & Propagation Conference (LAPC)*. IEEE, 2015, pp. 1–4.
- [36] M. Y. ElSalamouny and R. M. Shubair, "Novel design of compact low-profile multi-band microstrip antennas for medical applications," in *2015 Loughborough Antennas & Propagation Conference (LAPC)*. IEEE, 2015, pp. 1–4.
- [37] A. A. Ibrahim, J. Machac, and R. M. Shubair, "Compact uwb mimo antenna with pattern diversity and band rejection characteristics," *Microwave and Optical Technology Letters*, vol. 59, no. 6, pp. 1460–1464, 2017.
- [38] R. Shubair and A. Merri, "Convergence of adaptive beamforming algorithms for wireless communications," in *Proc. IEEE and IFIP International Conference on Wireless and Optical Communications Networks*, 2005, pp. 6–8.
- [39] J. An, G.-M. Wang, C.-X. Zhang, and H.-Y. Zeng, "Compact circularly polarized omnidirectional microstrip antenna," *Microwave and Optical Technology Letters*, vol. 51, no. 11, pp. 2643–2646, 2009.
- [40] K. Ray, R. Kulkarni, and B. K. Ramkrishnan, "Doa estimation in a multipath environment using covariance differencing and iterative forward and backward spatial smoothing," in *2008 International Conference on Recent Advances in Microwave Theory and Applications*. IEEE, 2008, pp. 794–796.
- [41] A. Hakam, M. Hussein, M. Ouda, R. Shubair, and E. Serria, "Novel circular antenna with elliptical rings for ultra-wide-band," in *2016 10th European Conference on Antennas and Propagation (EuCAP)*. IEEE, 2016, pp. 1–4.
- [42] M. I. Hussein, A. Hakam, M. Ouda, and R. M. Shubair, "Compact low-profile planar elliptical antenna for uwb applications," in *2016 10th European Conference on Antennas and Propagation (EuCAP)*. IEEE, 2016, pp. 1–2.
- [43] E. M. Al-Ardi, R. M. Shubair, and M. E. Al-Mualla, "Investigation of high-resolution DOA estimation algorithms for optimal performance of smart antenna systems," in *4th International Conference on 3G Mobile Communication Technologies*, Jan. 2003, pp. 460–464.
- [44] —, "Performance evaluation of direction finding algorithms for adaptive antenna arrays," in *10th IEEE International Conference on Electronics, Circuits and Systems, 2003. ICECS 2003. Proceedings of the 2003*, vol. 2, Dec. 2003, pp. 735–738 Vol.2.
- [45] J. Wiart, C. Dale, A. V. Bosisio, and A. Le Cornec, "Analysis of the influence of the power control and discontinuous transmission on rf exposure with gsm mobile phones," *IEEE Transactions on electromagnetic compatibility*, vol. 42, no. 4, pp. 376–385, 2000.
- [46] P. Bernardi, M. Cavagnaro, S. Pisa, and E. Piuze, "Power absorption and temperature elevations induced in the human head by a dual-band monopole-helix antenna phone," *IEEE Transactions on Microwave Theory and Techniques*, vol. 49, no. 12, pp. 2539–2546, 2001.
- [47] A. Gati, A. Hadjem, M.-F. Wong, and J. Wiart, "Exposure induced by wcdma mobiles phones in operating networks," *IEEE Transactions on wireless communications*, vol. 8, no. 12, pp. 5723–5727, 2009.
- [48] S. Kühn and N. Kuster, "Field evaluation of the human exposure from multiband, multisystem mobile phones," *IEEE Transactions on Electromagnetic Compatibility*, vol. 55, no. 2, pp. 275–287, 2012.
- [49] B. Xu, M. Gustafsson, S. Shi, K. Zhao, Z. Ying, and S. He, "Radio frequency exposure compliance of multiple antennas for cellular equipment based on semidefinite relaxation," *IEEE Transactions on Electromagnetic Compatibility*, vol. 61, no. 2, pp. 327–336, 2018.
- [50] D. G. Lopez, M. Ignatenko, and D. S. Filipovic, "Eigenmode prediction of high rf exposure frequency region inside vehicles," *IEEE Transactions on Electromagnetic Compatibility*, vol. 59, no. 1, pp. 43–47, 2016.
- [51] S. Ghosal, A. De, A. P. Duffy, and A. Chakrabarty, "Selection of dominant characteristic modes," *IEEE Trans Electromagn Compat*, pp. 1–10, 2019.
- [52] X.-Q. Zhu, Y.-X. Guo, and W. Wu, "Miniaturized dual-band and dual-polarized antenna for mban applications," *IEEE Trans. Antennas Propagat.*, vol. 64, no. 7, pp. 2805–2814, 2016.
- [53] B. J. DeLong, A. Kiourti, and J. L. Volakis, "A radiating near-field patch rectenna for wireless power transfer to medical

- implants at 2.4 ghz,” *IEEE Journal of Electromagnetics, RF and Microwaves in Medicine and Biology*, vol. 2, no. 1, pp. 64–69, 2018.
- [54] A. S. Poon, S. O’Driscoll, and T. H. Meng, “Optimal frequency for wireless power transmission into dispersive tissue,” *IEEE Trans. Antennas Propag.*, vol. 58, no. 5, pp. 1739–1750, 2010.
- [55] A. S. Poon, “Electromagnetic field focusing for short-range wireless power transmission,” in *Radio and Wireless Symposium (RWS), 2012 IEEE*. IEEE, 2012, pp. 115–118.
- [56] G. G. Bellizzi, L. Crocco, G. M. Battaglia, and T. Isernia, “Multi-frequency constrained sar focusing for patient specific hyperthermia treatment,” *IEEE Journal of Electromagnetics, RF and Microwaves in Medicine and Biology*, vol. 1, no. 2, pp. 74–80, 2017.
- [57] Y. Fan, J. Huang, T. Chang, and X. Liu, “A miniaturized four-element mimo antenna with ebg for implantable medical devices,” *IEEE Journal of Electromagnetics, RF and Microwaves in Medicine and Biology*, 2018.
- [58] S. Ghosal and S. R. B. Chaudhuri, “Analysis of a rectangular slot on a microstrip patch antenna with an equivalent circuit model,” in *Applied Electromagnetics Conference (AEMC), 2013 IEEE*. IEEE, 2013, pp. 1–2.
- [59] M. U. Khan, M. S. Sharawi, and R. Mittra, “Microstrip patch antenna miniaturisation techniques: a review,” *IET Microw., Antennas Propag.*, vol. 9, no. 9, pp. 913–922, 2015.
- [60] J.-Y. Sze and K.-L. Wong, “Slotted rectangular microstrip antenna for bandwidth enhancement,” *IEEE Trans. Antennas Propag.*, vol. 48, no. 8, pp. 1149–1152, 2000.
- [61] P. Juyal and L. Shafai, “Sidelobe reduction of tm<sub>12</sub> mode of circular patch via nonresonant narrow slot,” *IEEE Trans. Antennas Propag.*, vol. 64, no. 8, pp. 3361–3369, 2016.
- [62] D. Pozar, “A reciprocity method of analysis for printed slot and slot-coupled microstrip antennas,” *IEEE Trans. Antennas Propag.*, vol. 34, no. 12, pp. 1439–1446, 1986.
- [63] S. Ghosal, A. De, A. Chakrabarty, and R. M. Shubair, “Characteristic mode analysis of slot loading in microstrip patch antenna,” *IEEE APS/URSI Symp. 2018, Boston, USA*, 2018.
- [64] —, “Analysis of slot loading in elliptical patch- a characteristic mode approach,” *IEEE ANTEM 2018, Canada*, 2018.
- [65] R. Harrington and J. Mautz, “Theory of characteristic modes for conducting bodies,” *IEEE Trans. Antennas Propag.*, vol. 19, no. 5, pp. 622–628, 1971.
- [66] F. H. Lin and Z. N. Chen, “A method of suppressing higher-order modes for improving radiation performance of metasurface multiport antennas using characteristic mode analysis,” *IEEE Trans. Antennas Propag.*, 2018.
- [67] J. Zhao, Y. Chen, and S. Yang, “In-band radar cross section reduction of slot antenna using characteristic modes,” *IEEE Antennas Wireless Propag. Lett.*, 2018.
- [68] U. G. Matlab, “The mathworks,” *Inc., Natick, MA*, vol. 1992, 1760.
- [69] S. N. Makarov, *Antenna and EM Modeling with MATLAB*. Wiley-Interscience,, 2002.
- [70] H. ANSYS, “Ansoft corp., pittsburgh, pa,” 2015.